Self-Powered Nanodevice

DOI: 10.1002/anie.201104197

Fiber-Based Hybrid Nanogenerators for/as Self-Powered Systems in Biological Liquid**

*Caofeng Pan, Zetang Li, Wenxi Guo, Jing Zhu, and Zhong Lin Wang**

A goal of nanotechnology is to create nanosystems that are intelligent, multifunctional, super-small, extremely sensitive, and low power consuming. The search for sustainable power sources for driving such nanosystems is an emerging field in today's energy research,[1] and harvesting energy from multiple sources available in the environment is highly desirable for creating self-powered nanosystems.[2] For implanted nanodevices, such as a glucose sensor used to monitoring diabetes, it is rather challenging to power them since the solar energy is not available inside the body and thermal energy cannot be used because there is no temperature gradient. The only available energy in vivo is mechanical and biochemical energy. Nanogenerators (NGs) were demonstrated to convert low- ($\approx$Hz) and high-frequency ($\approx$50 kHz) mechanical energy into electricity by means of piezoelectric zinc oxide (ZnO) nanowires (NWs).[3] Following this landmark discovery, direct current (DC)[4] and alternative current (AC) NGs,[5] single-wire[6] and multi-nanowire arrays-based[7] NGs have been developed. On the other hand, biofuel cells have been demonstrated to convert biochemical energy into electricity by using active enzymes as catalyst and glucose as fuel.[8] We have previously demonstrated that biochemical and mechanical generators can work together to harvest multiple kinds of energy in bio-liquid, however, the two units were separately arranged on plastic substrate without integration, and the output was too low and the size was too large to be used for real applications.[2c] Here we demonstrate a flexible fiber-based hybrid nanogenerater (hybrid NG) consisting of a fiber nanogenerator (FNG) and a fiber biofuel cell (FBFC), which can be used in bio-liquid (such as blood) for energy harvesting. The FNG and FBFC are totally integrated on a single carbon fiber for the first time for simultaneously or independently harvesting mechanical and biochemical energy. In addition, the hybrid NG can also serve as a self-powered pressure sensor for detecting pressure variation in bio-liquid. Our fiber-based hybrid NG is an outstanding example of self-powered nanotechnology for applications in biological sciences, environmental monitoring, defense technology, and even personalized electronics.

A hybrid nanogenerater made up of a fiber nanogenerater (FNG) and a fiber biofuel cell (FBFC) is designed onto a carbon fiber. The design of the FNG is based on the textured ZnO NW film grown on the surface of the carbon fiber. The carbon fiber serves not only as the substrate on which the ZnO NW film is grown, but also as an electrode (noted as core electrode). In previous work we have fabricated a textured ZnO NW film by using physical vapor deposition.[9] The FNG was fabricated by etching the ZnO NW film at one end of the carbon fiber, contacting the top surface using silver paste and tape, and leading out two electrodes from the surface and the core electrodes (left-hand in Figure 1a). An FBFC, which is used for converting chemical energy from bio-fluid such as glucose/blood into electricity,[1b] is fabricated at the other end of the carbon fiber (Figure 1a). A layer of soft epoxy polymer is coated on the carbon fiber as an insulator, then two gold electrodes are patterned onto it and coated with carbon nanotubes (CNTs), followed by immobilization of glucose oxidase (GOx) and laccase to form the anode and cathode, respectively. In comparison to conventional biofuel cells[10] and miniature biofuel cells,[11] the FBFCs described here were integrated with the NG (or nanodevices) on an individual carbon fiber, forming a self-powered nanosystem. And the size of the FBFCs shrank a lot due to eliminating the separator membrane and mediator. For easy handling and fabrication, we created our hybrid NG on individual carbon fibers, and our measurements were performed on a bundle of (ca. 1000) carbon fibers.

The performance of the hybrid NG is characterized by measuring the short-circuit current I_{sc} and the open-circuit voltage V_{oc}. The FBFC outputs are given as V_{FBFC} and I_{FBFC}, the AC FNG outputs as V_{FNG} and I_{FNG}, and the hybrid NG outputs as V_{HNG} and I_{HNG}. When the hybrid NG is immersed into bio-liquid containing glucose, the FBFC generates a DC output. A typical FBFC output is shown in Figure 2a and b with I_{FBFC} of ca. 100 nA and V_{FBFC} of ca. 100 mV. When a pressure is periodically applied to the bio-liquid, the FNG starts to generate an AC output. The general output of V_{FNG} is 3.0 V at an output current of $I_{FNG} = 200$ nA (Figure 2c and d) for an FNG made of ca. 1000 carbon fibers, and the corresponding current density is 0.06 $\mu A\,cm^{-2}$.

By integrating the AC FNG and DC FBFC, a hybrid NG is obtained with the output close to the sum of the FBFC and the FNG (Figure 2e and f). The shape and frequency of the AC FNG output are the same before and after the hybrid-

[*] Dr. C. Pan, Z. Li, W. Guo, Prof. Z. L. Wang
School of Materials Science and Engineering
Georgia Institute of Technology, Atlanta, GA 30332-0245 (USA)
E-mail: zlwang@gatech.edu
Homepage: http://www.nanoscience.gatech.edu/zlwang
Prof. J. Zhu
Beijing National Center for Electron Microscopy
Department of Material Science and Engineering
Tsinghua University, Beijing 100084 (P.R. China)

[**] This research was supported by NSF (DMS 0706436, CMMI 0403671), DARPA (HR0011-09-C-0142, Program manager, Dr. Daniel Wattendorf), BES DOE (DE-FG02-07ER46394). The authors thank Prof. C. M. Lieber for stimulating discussions and Dr. Yan Zhang and Sihong Wang for technical assistance.

Supporting information for this article is available on the WWW under http://dx.doi.org/10.1002/anie.201104197.

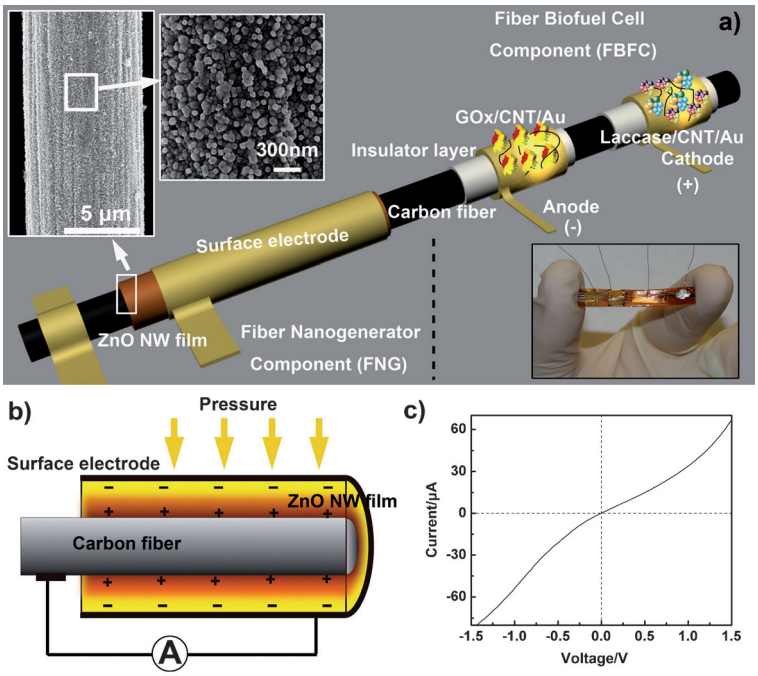

Figure 1. Design of a single fiber-based hybrid nanogenerator for simultaneous harvesting of biochemical and mechanical energy from an external force or pressure applied to a liquid. a) Schematic 3D representation of the hybrid nanogenerator. The inserts in the upper left are SEM images of a textured ZnO NW film grown around a carbon fiber composed of densely packed ZnO NW to form a continuous textured film. A digital image of the device is shown at the lower corner. b) Working principle of the FNG. +/− signs indicate the polarity of the local piezoelectric potential created on the inner and outer surfaces of the ZnO NW film as a result of the applied pressure. c) *I*–*V* characteristic of the FNG for mechanical energy harvesting showing the presence of Schottky barriers at its two ends.

ization process, only the base line shifts from zero to the FBFC output. The peak value of the hybrid NG open-circuit voltage, V_{HNG}, is ± 3.1 V when they are in series; the peak value of the short-circuit current, I_{HNG}, is 300 nA and −100 nA, when they are in parallel. In addition, methods have been developed to rectify the AC NG output to obtain a DC signal and to integrate with the DC output of the FBFC to give an overall enhancement in DC output.[7b]

The fiber-based hybrid NG can also work as a self-powered nanosystem when FNG and FBFC are connected in series to form a loop (see Figures S3b and S4 in the Supporting Information). In such a case, the FNG effectively works as a piezoelectric sensor ("load"), and the FBFC plays the role of the power source that "drives" the FNG (Figure 3a), forming a self-powered system for monitoring pressure variation in a bio-liquid. The pressure is applied periodically at an interval of 1.9 s for an extended period of 0.7 s. The base-line current in the circuit is about 128 nA when the bio-liquid is under ambient atmosphere (labeled "d" in Figure 3b). When pressure is applied, a distinct peak in the measured current rapidly arises (labeled as "e" in Figure 3b) and the current increases to a new plateau value which remains constant while pressure is still applied (labeled as "f" in Figure 3b). When the pressure is released, a rapid and obvious decrease in current is detected (labeled as "g" in Figure 3b). A connection polarity reversion test was carried out, which shows that the

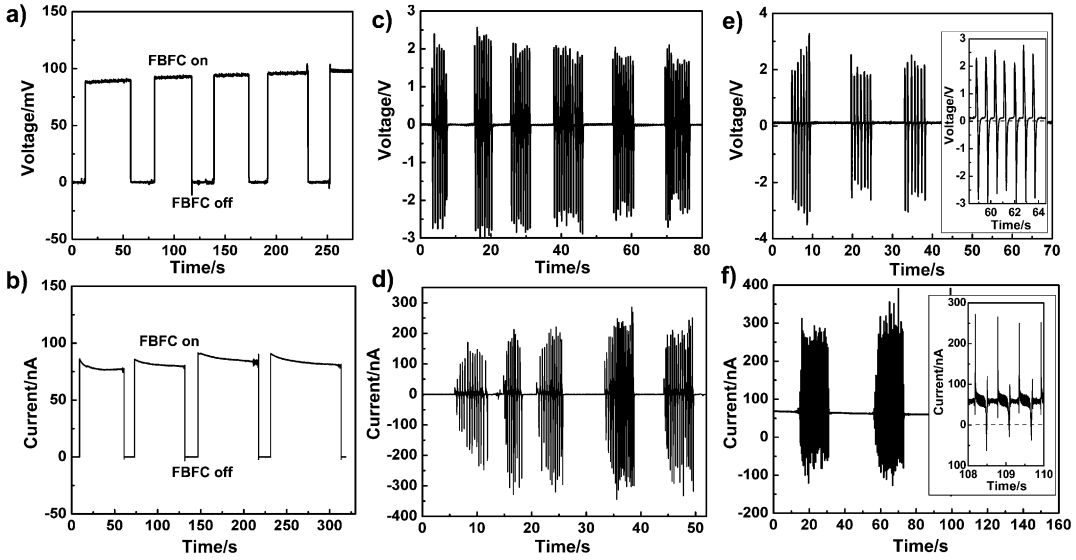

Figure 2. Typical output signals of the hybrid nanogenerator. a,b) V_{FBFC} and I_{FBFC} of the fiber biofuel cells resulting from conversion of chemical energy in glucose into electricity. c,d) V_{FNG} and I_{FNG} of the flexible fiber NG as driven by an applied pressure. e) Open-circuit voltage of the hybrid NG when the FNG and the FBFC are connected in series. f) Short-circuit current of the hybrid NG when the FNG and the FBFC are connected in parallel. The insets in (e) and (f) are enlarged plots of the corresponding outputs showing the details of the signals; dashed lines indicate the zero-output line.

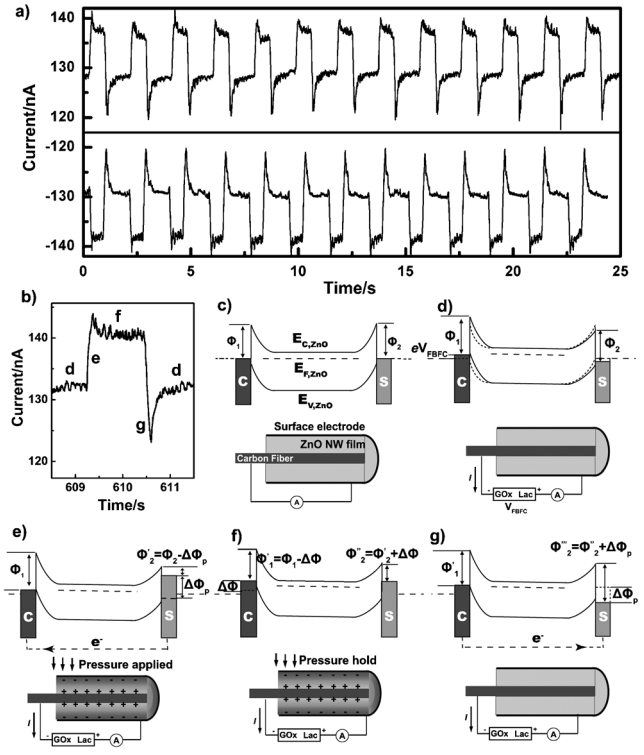

Figure 3. Function of the hybrid nanogenerator as a self-powered pressure measurement nanosystem in bio-liquid. a) Electrical current measured by connecting the FBFC and FNG in series, where the FBFC functions as the power source and the FNG as the sensor. A pressure of 1.35 P_0 is applied periodically at 1.9 s period with a pressure hold for 0.7 s. b) Enlarged plot of a single output period as shown in (a). The four processes labeled as "d", "e", "f", and "g" correspond to panels (d)–(g), respectively. c) Energy band diagram (upper) and the corresponding short-circuit diagram (lower) of a strain-free ZnO FNG having two Schottky contacts with a metal electrode on the outer surface (S) and a carbon fiber at the core (C). The dashed line is the Fermi level (E_F) of the electrodes; E_C and E_V are the ZnO conduction and valence bands, respectively; Φ_1 and Φ_2 are the Schottky barrier height (SBHs) at the two contacts, respectively. d–g) Energy band diagrams (upper) and the corresponding circuit diagrams (lower) of the FNG (as the sensor) that is driven by the FBFC and corresponding to the "d", "e", "f", and "g" processes labeled in (b). In (d) the FNG is at ambient pressure; dashed and solid lines represent the band diagrams before and after applying the bias provided by FBFC, respectively, with a relative shift of the Fermi levels by eV_{FBFC} at the two contacts. Case (e) is the same as in (d) but with a pressure being applied to the FNG before the system reaches an equilibrium; the color grade in the ZnO film represents the distribution of piezopotential drop of $\Delta\Phi_p$. Case (f) is the same as in (e) except a constant pressure is applied and the system reaches an equilibrium. The electrons flow from S to C results in a shift of the Fermi levels by $\pm\Delta\Phi$ (ideally $\Delta\Phi = 1/2\Delta\Phi_p$), respectively. Case (g) is the same as in (f) except the pressure applied to the FNG is released. The piezopotential disappears and there is a relative drop in Fermi level by $\Delta\Phi_p$ generating a relative negative current peak as the electrons flow back to reach equilibrium.

output signal is reversible (lower part in Figure 3a), as expected.

The variation of the resistance of the ZnO sensor was attributed to a combination of bulk resistance change (piezoresistance) and the piezoelectronic effect, as discussed in previous work.[12] The piezoresistive effect, which differs from the piezoelectronic effect, is a change in resistance of a semiconductor due to applied mechanical stress owing to a change in bandgap and local carrier density. The changing of the resistance can be obtained through Equation (1):

$$\frac{\Delta R}{R} = \pi_l \Delta\sigma_l + \pi_t \Delta\sigma_t \text{[13]} \quad (1)$$

where R is the resistance, ΔR is the change of resistance, π_l and π_t are the longitudinal and transverse piezoresistive effect coefficient, and $\Delta\sigma_l$ and $\Delta\sigma_t$ are the changes in stress applied to the longitudinal and transverse direction of ZnO NWs.

In the present work, $\Delta\sigma_t$ is 0.35 P_0, $\Delta\sigma_l$ is sufficiently small to be ignored, and $\Delta R/R$ is ca. 10%. If the piezoresistive effect were the dominant contributor, the piezoresistive coefficient π would be 285000×10^{-11} Pa^{-1}, which is several orders of magnitude higher than reported values.[14] That means the piezoresistive effect cannot be the dominant contributor for our observed result. In reference to our many studies of ZnO, the piezoelectric effect is the dominant contributor to the resistance change, which occurs right at the contact with the electrode.

Our results can be explained using the energy band diagram as shown in Figure 3c–g. The processes shown in Figure 3c–g which bear reference to our discussion are correspondingly labeled in Figure 3b as "c"–"g". The ZnO NWs array used in our experiments were densely grown on the carbon fiber to form a textured film. A strain-free ZnO NW usually has non-symmetric Schottky contacts at its two ends with different Schottky barrier heights (SBH; noted as Φ_1 and Φ_2, respectively) (Figure 1c). When the FNG is connected with an FBFC in series (Figure 3d), a bias was applied to the FNG owing to the output voltage of the FBFC. When the carbon fiber electrode is connected to the anode of the FBFC, the Fermi levels at the two ends differ by eV_{FBFC}, where V_{FBFC} is the output bias generated by the FBFC (Figure 3d).

When the ZnO NW film is subjected to a compressive strain, a piezoelectric field is created in the ZnO NW film due to polarization of ions in the crystal, with the positive piezopotential (V^+) at the carbon fiber electrode side (left-hand side in Figure 3e,f), and the corresponding negative side (V^-) at the surface electrode side (right-hand side in Figure 3e,f). These non-mobile piezoelectric ionic charges remain in the ZnO NW film for an extended period of time without being fully screened by the free carriers as long as the strain is preserved and doping level is low. As a result, the conduction band and Fermi level of the electrode at the right-hand side is raised by $\Delta\Phi_p = e(V^+ - V^-)$ with respect to the electrode on the left-hand side, and electrons will flow from the right-hand side electrode to the left-hand side electrode through an external load that is the FNG in the current case, showing a sharp peak in the measured current (Figure 3e). Because of the Schottky barrier, these electrons are accumulated around the interfacial region between the left-hand side electrode and the wire, thus raising the local Fermi level; this process continues until the potential created by the accumulated electrons balances the piezopotential, and the Fermi

levels of the two electrodes reach a new equilibrium, with a SBH $\Phi'_1 = \Phi_1 - \Delta\Phi < \Phi_1$ (Figure 3 f). As a result, experimentally, the current in the circuit spontaneously increases from 128 nA to 135 nA, as labeled with "f" in Figure 3 b.

Alternatively, when the compressive strain on the FNG is released the immediate disappearance of the piezopotential lowers the Fermi level of the right-hand electrode by $\Delta\Phi_p$ and the electrons flow back from the left-hand electrode through the external circuit to the right-hand electrode (Figure 3 g), creating an electric pulse in the opposite direction and thus returning the system to its original state. The process ends when the Fermi levels of the two sides reach equilibrium again.

Theoretical calculations have shown that, within the elastic linear mechanics regime, the output voltage of a single nanowire is proportional to the magnitude of its deformation.[15] An increase on the pressure applied to the ZnO NW film leads to an increase of piezopotential $\Delta\Phi_p$, resulting in a higher current jump in the circuit. Current as a function of applied pressure is shown in Figure 4 a. As the applied pressure increases from ambient atmosphere P_0 to $1.05\,P_0$, $1.15\,P_0$, $1.25\,P_0$, and then $1.35\,P_0$, the response current increases from 128 nA to 135 nA, that is, by roughly 7 % (Figure 4 b). When such a small pressure is applied, the response increases linearly, with a slope of ca. 19.2, following a relationship $\Delta I/I = 0.192\,P/P_0 - 0.183$ (Figure 4 b). The sensitivity for the pressure measurement demonstrated here is 1.35 %. This means that we can monitor the pressure in a liquid, such as blood pressure in blood vessel, by monitoring the current change in the circuit. This is a self-powered hematomanometer.

The self-powered technique presented in Figure 4 c and d is developed to detect the pressure (or force) variation by changing the frequency, interval time, and holding time of pressure application. Such study is intended for monitoring tiny pressure variations (or mechanical agitations) in human blood vessel. The response of the self-powered nanosystem on different interval time under periodic pressure $P = 1.35\,P_0$ is recorded in Figure 4 c; the response on holding time is recorded in Figure 4 d. A connection polarity reversion test is carried out for the pressure monitoring process, and the reversion in output signal is apparent. From the current jump in the circuit we can calculate the pressure value from $P = (5.2\Delta I/I + 0.95)\,P_0$.

Self-powered nanodevices such as the one described may have potential applications for health care monitoring.[16] As is well-known the human heart generates a periodic pulse pressure, which is a complex time-dependent and nonlinear signal reflecting the fluctuation of one's motion and health situation, resulting in a fluctuation in blood pressure.[17] A quantitative measurement of such a pressure signal could provide important information for health care and medical diagnostics.[18] Our self-powered hybrid nanosystem has the potential to be used for such purpose.

In summary, we have presented a fiber-based hybrid nanogenerator consisting of a fiber nanogenerator and a fiber

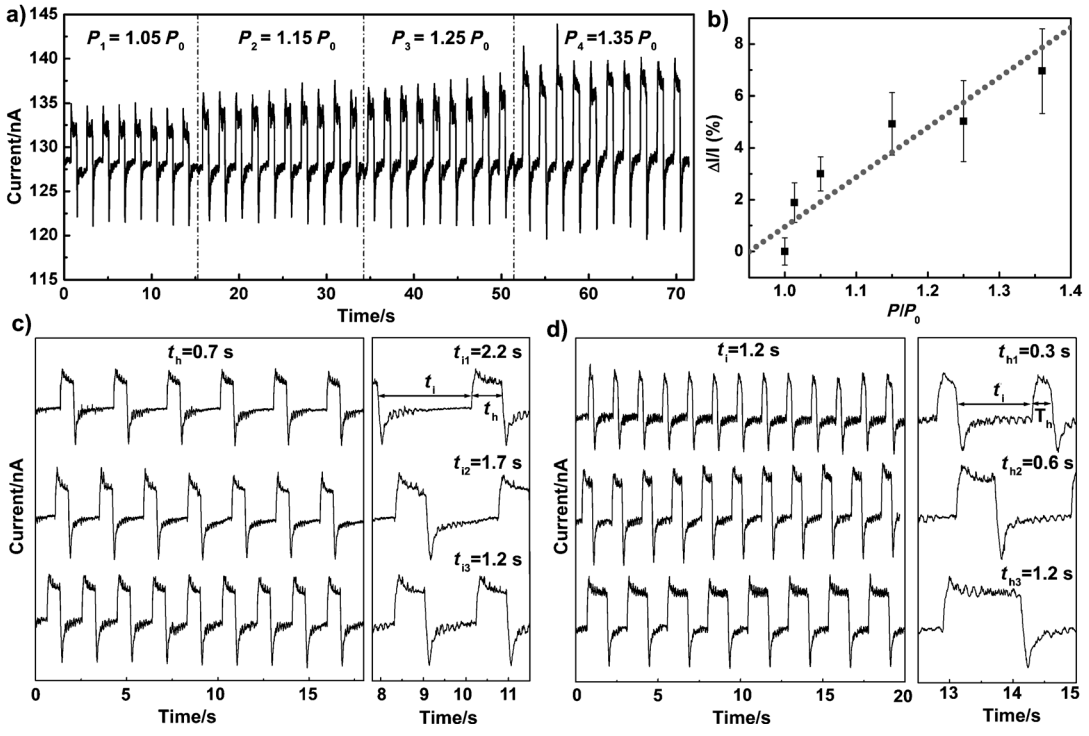

Figure 4. Pressure measurement in bio-liquid by using a hybrid nanogenerator as a self-powered system. a) Response of the hybrid NG system to periodically applied pressure. b) Plot of the statistically measured steady current from (a) as a function of applied pressure showing a linear relationship. c) Measured current from the hybrid NG on varying the period at which the pressure is applied while the time interval of holding the pressure is kept constant. d) Measured current from the hybrid NG on varying the holding time while the interval during which the pressure is off is kept constant. The plot at the right-hand side of (c) and (d) are enlarged plots for one cycle of output current.

biofuel cell, which can be used in bio-liquid for converting mechanical and biochemical energy into electricity. On immersion of the hybrid NG into a bio-liquid the BFC generates a DC output of ca. $V_{FBFC} = 100$ mV and $I_{FBFC} = 100$ nA. When a periodic pressure is applied onto the bio-liquid, the FNG operates under a compressive strain generating an AC output with a peak value of $V_{FNG} = \pm 3$ V and $I_{FNG} = \pm 200$ nA. The hybrid NG allows simultaneous harvesting of mechanical and biochemical energy with great potential for the powering of in vivo nanodevices. Integrating hybrid NGs with nanosensors and a radiofrequency unit for data transmission could provide a self-powered, independent, and wireless system for medical monitoring. Furthermore, hybrid NG can operate as a "self-powered" sensor to measure pressure variations in bio-liquid, where the FNG serves as the pressure sensor and the FBFC is the power source. Such system can be used not only for monitoring blood pressure, but also for monitoring the operation of gas/water/oil pipes. Our hybrid nanogererator is likely to have applications in implantable biomedical devices and environmental/infrastructure monitoring.

Received: June 17, 2011
Revised: September 1, 2011
Published online: September 28, 2011

Keywords: biofuel cells · hybrid nanogenerator · personalized electronics · self-powered nanodevice

[1] a) Z. L. Wang, *Sci. Am.* **2008**, *298*, 82–87; b) C. F. Pan, Y. Fang, H. Wu, M. Ahmad, Z. X. Luo, Q. A. Li, J. B. Xie, X. X. Yan, L. H. Wu, Z. L. Wang, J. Zhu, *Adv. Mater.* **2010**, *22*, 5388–5392; c) C. F. Pan, H. Wu, C. Wang, B. Wang, L. Zhang, Z. D. Cheng, P. Hu, W. Pan, Z. Y. Zhou, X. Yang, J. Zhu, *Adv. Mater.* **2008**, *20*, 1644–1648; d) B. Z. Tian, X. L. Zheng, T. J. Kempa, Y. Fang, N. F. Yu, G. H. Yu, J. L. Huang, C. M. Lieber, *Nature* **2007**, *449*, 885–U888.

[2] a) C. Xu, Z. L. Wang, *Adv. Mater.* **2011**, *23*, 873–877; b) C. Xu, X. D. Wang, Z. L. Wang, *J. Am. Chem. Soc.* **2009**, *131*, 5866–5872; c) B. J. Hansen, Y. Liu, R. S. Yang, Z. L. Wang, *Acs Nano* **2010**, *4*, 3647–3652; d) Y. Hu, Y. Zhang, C. Xu, L. Lin, R. L. Snyder, Z. L. Wang, *Nano Lett.* **2011**, *11*, 2572–2577.

[3] a) Z. L. Wang, J. H. Song, *Science* **2006**, *312*, 242–246; b) Z. Z. Shao, L. Y. Wen, D. M. Wu, X. A. Zhang, S. L. Chang, S. Q. Qin, *Appl. Surf. Sci.* **2011**, *257*, 4919–4922.

[4] a) X. D. Wang, J. H. Song, J. Liu, Z. L. Wang, *Science* **2007**, *316*, 102–105; b) Y. Xi, D. H. Lien, R. S. Yang, C. Xu, C. G. Hu, *Phys. Status Solidi RRL* **2011**, *5*, 77–79.

[5] a) C. E. Chang, V. H. Tran, J. B. Wang, Y. K. Fuh, L. W. Lin, *Nano Lett.* **2010**, *10*, 726–731; b) Y. F. Hu, Y. Zhang, C. Xu, G. A. Zhu, Z. L. Wang, *Nano Lett.* **2010**, *10*, 5025–5031; c) G. A. Zhu, R. S. Yang, S. H. Wang, Z. L. Wang, *Nano Lett.* **2010**, *10*, 3151–3155; d) K. J. Kim, D. Mandal, S. Yoon, *Macromol. Rapid Commun.* **2011**, *32*, 831–837.

[6] R. S. Yang, Y. Qin, L. M. Dai, Z. L. Wang, *Nat. Nanotechnol.* **2009**, *4*, 34–39.

[7] a) X. Y. Wang, K. Kim, Y. M. Wang, M. Stadermann, A. Noy, A. V. Hamza, J. H. Yang, D. J. Sirbuly, *Nano Lett.* **2010**, *10*, 4901–4907; b) S. Xu, B. J. Hansen, Z. L. Wang, *Nat. Commun.* **2010**, *1*, 93–97.

[8] a) N. Mano, F. Mao, A. Heller, *J. Am. Chem. Soc.* **2003**, *125*, 6588–6594; b) N. Mano, F. Mao, A. Heller, *J. Am. Chem. Soc.* **2002**, *124*, 12962–12963; c) I. Willner, V. Heleg-Shabtai, R. Blonder, E. Katz, G. L. Tao, A. F. Buckmann, A. Heller, *J. Am. Chem. Soc.* **1996**, *118*, 10321–10322.

[9] Z. T. Li, Z. L. Wang, *Adv. Mater.* **2011**, *23*, 84–89.

[10] a) R. A. Bullen, T. C. Arnot, J. B. Lakeman, F. C. Walsh, *Biosens. Bioelectron.* **2006**, *21*, 2015–2045; b) J. R. Rao, G. J. Richter, F. Vonsturm, E. Weidlich, *Bioelectrochem. Bioenerg.* **1976**, *3*, 139–150; c) G. T. R. Palmore, H. Bertschy, S. H. Bergens, G. M. Whitesides, *J. Electroanal. Chem.* **1998**, *443*, 155–161.

[11] a) A. Heller, *Phys. Chem. Chem. Phys.* **2004**, *6*, 209–216; b) S. Shleev, V. Coman, R. Ludwig, W. Harreither, D. Haltrich, L. Gorton, T. Ruzgas, *Fuel Cells* **2010**, *10*, 9–16.

[12] J. Zhou, P. Fei, Y. D. Gu, W. J. Mai, Y. F. Gao, R. Yang, G. Bao, Z. L. Wang, *Nano Lett.* **2008**, *8*, 3973–3977.

[13] S. M. Sze, *Semiconductor Sensors*, Wiley-Interscience, New York, **1994**.

[14] a) T. T. T. Nghiem, V. Aubry-Fortuna, C. Chassat, A. Bosseboeuf, P. Dollfus, *Mod. Phys. Lett. B* **2011**, *25*, 995–1001; b) P. D. Yang, R. R. He, *Nat. Nanotechnol.* **2006**, *1*, 42–46; c) the unit of the piezoresistive coefficient is commonly given as 10^{-11} Pa^{-1}, and most of the data reported on piezoresistive coefficients are for Si and Ge. The highest "giant piezoresistive coefficient" reported is 3100×10^{-11} Pa^{-1} (see Ref. [14b]). Here, we consider this highest piezoresistive coefficient of Si as a reference since little report is found on ZnO piezoresistive coefficients.

[15] a) Y. Gao, Z. L. Wang, *Nano Lett.* **2007**, *7*, 2499–2505; b) Y. Zhang, Y. Liu, Z. L. Wang, *Adv. Mater.* **2011**, *23*, 3004–3013.

[16] a) J. A. Chirinos, R. Townsend, *J. Am. Coll. Cardiol.* **2010**, *56*, 744–744; b) A. Mahmud, J. Feely, *Hypertension* **2003**, *41*, 183–187.

[17] a) I. B. Wilkinson, I. R. Hall, H. MacCallum, I. S. Mackenzie, C. M. McEniery, B. J. van der Arend, Y. E. Shu, L. S. MacKay, D. J. Webb, J. R. Cockcroft, *Arterioscler. Thromb. Vasc.* **2002**, *22*, 147–152; b) A. M. Dart, B. A. Kingwell, *J. Am. Coll. Cardiol.* **2001**, *37*, 975–984.

[18] J. J. Shu, Y. Sun, *Complement. Ther. Med.* **2007**, *15*, 190–198.

